(Received 21 September 2025, Accepted 15 November 2025, Scheduled 1 December 2025)

Broadband Sequential Load Modulation Power Amplifier for Expanding Design Space

Jiadong Yu[1], Jingchang Nan[2,*], and Heyang Sun[1]

[1] School of Electronics and Information Engineering, Liaoning University of Engineering and Technology, Liaoning, China
[2] School of Electronics and Information Engineering, Liaoning University of Engineering and Technology, Henan, China

ABSTRACT: This study proposes an extended design methodology for sequential load-modulated balanced amplifiers (SLMBAs), centered on regulating the impedance characteristics of balanced amplifiers (BAs) through continuous F^{-1} class control amplifiers (CA). By expanding the load operating range of CAs at the second harmonic, the flexibility of high-efficiency designs is effectively enhanced. Theoretical analysis demonstrates that this load modulation mechanism overcomes the structural limitations of conventional LMBA, enabling high-efficiency power amplification across a wide frequency range and under conditions of large output power back-off (OPBO). Based on this architecture, an SLMBA prototype operating from 2.0 to 3.7 GHz was developed. Test results indicate that in saturated and 8 dB OPBO conditions, the drain efficiency (DE) reached 55.2%–68.7% and 46.8%–59.0%, respectively. When being fed with an LTE signal featuring a 100 MHz bandwidth and 8 dB PAPR, the average DE across the entire bandwidth ranged from 49.2% to 58.3%, with an adjacent channel leakage power ratio (ACPR) exceeding -35 dBc.

1. INTRODUCTION

Against the backdrop of the rapid advancement of fifth-generation (5G) communication systems, achieving the goals of high data rates, wide signal bandwidths, and high energy efficiency presents critical challenges for the design of radio frequency power amplifiers (PAs). One of the core challenges lies in the requirement that PAs maintain sufficiently high efficiency even at significantly reduced output power levels (large output power back-off, OPBO) when transmitting modulated signals with high peak-to-average power ratio (PAPR) characteristics [1, 2].

To address the need for PAs to maintain high efficiency at high OPBO levels, various efficiency-enhancing techniques have been developed, with load modulation [3] technology being a prominent example. Among them, load-modulated balanced amplifiers (LMBAs) [4–12] have received extensive research attention. The recently proposed sequential LMBA (SLMBA) [10] adopts a reverse operating mode, in which the carrier amplifier (CA) serves a role as the carrier, and the balanced amplifier (BA) functions as a peak amplifier. SLMBA has the potential to achieve a wider bandwidth than traditional LMBA, as its load modulation process is confined to the peak amplifier branch, simplifying the design of wideband matching networks — only requiring separate load conditions for the carrier or peak amplifier. Based on this reverse LMBA framework, other high-performance designs such as the pseudo-Doherty LMBA [12] and asymmetric LMBA [13] have also been validated.

Both SLMBA and pseudo-Doherty LMBA designs face a critical requirement: the load modulation trajectory of the BA must be purely resistive to ensure optimal power combination and maximize OPBO efficiency. However, practice has shown that maintaining a constant resistive fundamental load termination under wideband operating conditions is highly challenging. This difficulty limits design flexibility and hinders further performance improvements of the SLMBA scheme.

This paper proposes a new scheme aimed at overcoming the limitations of existing SLMBA designs based on time-domain waveform analysis of the continuous-mode (CM) amplifier topology. This scheme innovatively adopts a continuous F^{-1} class topology as the carrier amplifier (CA) to modulate the impedance trajectory of the balanced amplifier (BA). In the proposed SLMBA architecture, the load modulation process is realized by configuring the second harmonic load reactance of the CA to inject different fundamental current components into the BA. This mechanism effectively expands the basic design space of the BA.

2. THEORETICAL ANALYSIS

2.1. CA With Second-Harmonic Manipulation

SLMBA differs from the original LMBA in that the BA is designed as a Class C amplifier for peak power amplification, while the CA is designed as an AB/B-class amplifier for carrier power amplification. The general schematic diagram of the SLMBA structure with RF input is shown in Fig. 1(a). At low power input, the CA is turned on, and the BA is in the off state, with the output power provided solely by the CA. When high power is input, BA begins to conduct; CA remains saturated; and CA begins to modulate the load of BA. The three amplifiers in the SLMBA can be modeled using ideal current

* Corresponding author: Jingchang Nan (nanjingchang@lntu.edu.cn).

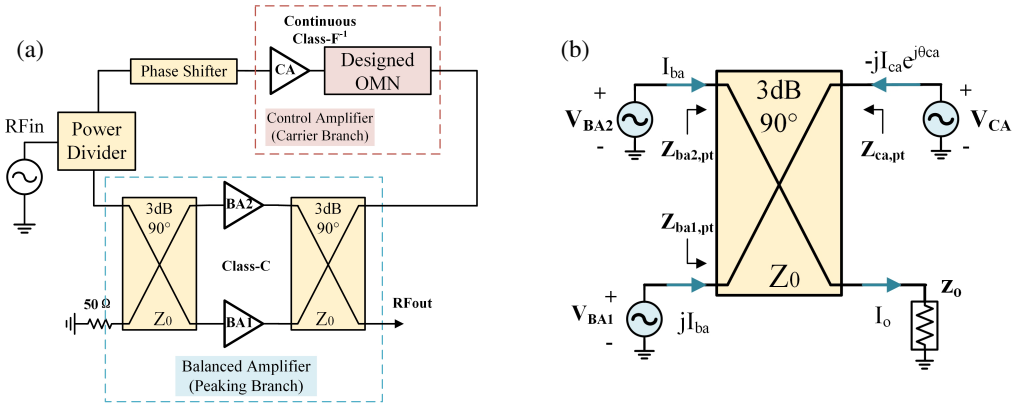

FIGURE 1. (a) Basic structure of SLMBA. (b) Theoretical block diagram of output power analysis.

sources connected to the output-end orthogonal couplers, as shown in Fig. 1(b). According to the theory of SLMBA proposed in [10, 12], the port impedance of BA can be expressed as

$$Z_{\text{ba1,pt}} = Z_{\text{ba2,pt}} = Z_{\text{ba,pt}} = Z_0\left(1+\sqrt{2}\frac{I_{\text{ca}}}{I_{\text{ba}}}e^{j\theta_{\text{ca}}}\right) \quad (1)$$

where Z_0 is the characteristic impedance of the coupler. $I_1 = jI_{\text{ba}}$ and $I_2 = I_{\text{ba}}$ indicate two identical BA signals. Due to the effect of the input coupler, the output currents have the same amplitude but a phase difference of 90°. The control path CA current is represented as $I_3 = -jI_{\text{ca}}e^{j\theta_{\text{ca}}}$. It can be seen that when the output signal of CA is injected into the isolation port of the output orthogonal coupler, the apparent impedance of the transistor pair in BA is controlled by the amplitude and phase of CA. This is determined by the characteristics of the orthogonal coupler. Ref. [14] provides the conclusion on phase shift when $\theta_{\text{ca}} = 0$, and the modulation impedance of BA is further simplified to (2).

$$Z_{\text{ba1,pt}} = Z_{\text{ba2,pt}} = Z_{\text{ba,pt}} = Z_0\left(1+\sqrt{2}\frac{I_{\text{ca}}}{I_{\text{ba}}}\right) \quad (2)$$

$$Z_{\text{ca,pt}} = Z_0 \quad (3)$$

The CA load is constant at Z_0, so CA and BA can be designed separately, greatly simplifying the implementation of broadband, rollback SLMBA. Due to the constant injection of CA signals, the BA load modulation trajectory is on the real axis [11, 12]. However, the fixed impedance terminal used to achieve this broadband operation is difficult, resulting in suboptimal performance of existing SLMBAs.

To expand the design space and address the bandwidth limitations of SLMBA, this paper proposes an SLMBA structure. As shown in Fig. 1(a), this structure provides a wider design space for CA and BA. In this architecture, the carrier branch uses a continuous F^{-1} class PA, which is reanalyzed based on its intrinsic drain voltage and current waveforms. The appropriate operation of the second harmonic load impedance Z_{ca} not only generates different time-domain current waveforms but also alters the time-domain drain voltage waveform. This provides a solution that can further expand the efficient CA design space by manipulating the second harmonic, enabling it to surpass continuous F^{-1}-class operation.

To quantify the performance improvement, parameter k_2 is introduced in [15], defined as the ratio of the second harmonic component to the fundamental component of the CA drain voltage, i.e., $k_2 = V_{\text{ca}}[2]/V_{\text{ca}}[1]$. It is assumed that the third harmonic terminates at a short circuit. Based on the analysis in [16, 17], the generalized CA drain voltage-current waveform can be expressed as

$$v_{d,\text{ca}}(\theta, k_2) = V_{\text{dc,ca}} - v_{\text{ca}}[1](\cos\theta + k_2\cdot\cos 2\theta) \quad (4)$$

$$i_{d,\text{ca}}(\theta) = \begin{cases} I_{\max,\text{ca}}\cos\theta - \left(\frac{4I_{\max,\text{ca}}}{3\pi}\cos 2\theta \right. \\ \left. -\frac{2\delta(k_2)k_2V_{\text{dck,ca}}}{\text{imag}(Z\text{ca,2nd})}\sin 2\theta\right), \\ -\frac{\pi}{2} < \theta < \frac{\pi}{2} \\ 0, \quad -\pi < \theta < -\frac{\pi}{2}, \quad \frac{\pi}{2} < \theta < \pi \end{cases} \quad (5)$$

where $I_{\max,\text{ca}}$ is the maximum current limit of the CA device; $V_{\text{dc}k,\text{ca}} = (V_{\text{dc,ca}} - V_{\text{knee,ca}})$; $V_{\text{dc,ca}}$ and $V_{\text{knee,ca}}$ are the drain supply voltage and the knee voltage of the device, respectively; $\delta(k_2)$ is the voltage gain function, which can be expressed according to the analysis in [15].

$$\delta(k_2) = \begin{cases} \frac{-1}{k_2+\frac{1}{8\cdot k_2}}, & \text{if } k_2 \le -\frac{1}{4} \\ \frac{1}{1+k_2}, & \text{if } -\frac{1}{4} \le k_2 \le 0 \end{cases} \quad (6)$$

As shown in Fig. 2, the waveforms of the drain voltage and current of the CA are plotted. It can be seen that the drain voltage waveform remains unchanged with variations in $Z_{\text{ca,2nd}}$, while the drain current waveform remains unchanged with different values of k_2. Therefore, the continuity of the fundamental and second harmonic load impedances can be relaxed from the strict requirements of the continuous F^{-1} class, thereby expanding the design space. Since the proposed SLMBA can be described based on the normalized input drive level β, we define β_{bo} as the input drive level corresponding to OBO [14, 16], where $0 \le \beta \le 1$. Based on the analysis in [18], the second harmonic relationship of CA is determined as shown in (7); the admittance form of the fundamental impedance of CA is given by Equation (8); and the k_2 value is preferably selected within

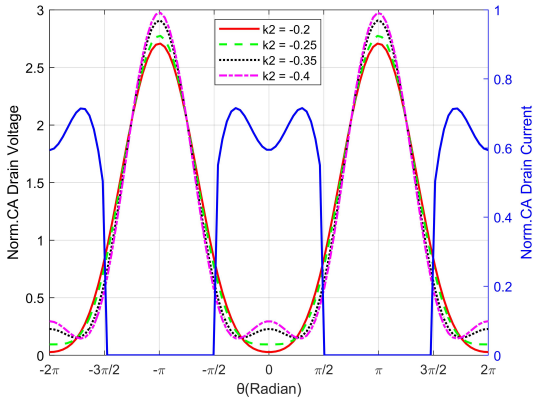

FIGURE 2. Normalized drain voltage (colored curve) and current (blue curve) waveforms with different k_2 values, namely, $k_2 = -0.20$, -0.25, -0.35, and -0.40.

the range $[-0.35, -0.20]$ to provide a good trade-off among voltage level at peak, ripple at minimum, and bandwidth expansion in the high-efficiency design space.

$$Z_{\text{ca,2nd}}^{\text{lim}} \approx \pm j \cdot \frac{8\delta(k_2) \cdot k_2 \cdot V_{\text{dck,ca}}}{I_{\text{max,ca}}} \tag{7}$$

$$Y_{\text{ca,1st}} = \left(\frac{1}{2} - \frac{8}{9\pi^2}\right)\frac{I_{\text{max,ca}}}{V_{\text{dck,ca}}}\frac{1}{\delta(k_2)} - j \cdot \frac{8}{3\pi}\frac{k_2}{\text{imag}(Z_{\text{ca,2nd}})} \tag{8}$$

2.2. BA Behavior Analysis

When the input power level β continuously increases from the OBO level β_{bo}, the BA begins to run. To better analyze the performance of the BA, its behavior was studied at peak power levels, where both the CA and BA operate in a saturated state at $\beta = 1$. The fundamental port impedance of the BA at saturation can be calculated as

$$\begin{aligned} Z_{\text{ba,pt,1st}} &= Z_0\left(1 + \sqrt{2}\frac{i_{\text{ca}}[1]}{i_{\text{ba}}[1]}\right) \\ &= Z_0\left(1 + \sqrt{2}\left(\frac{1}{2} - \frac{8}{9\pi^2}\right)\cdot\frac{1}{\sigma}\cdot\frac{I_{\text{max,ca}}}{I_{\text{max,ba}}}\right. \\ &\quad \left. - j \cdot \frac{8\sqrt{2}}{3\pi}\cdot\frac{1}{\sigma}\cdot\frac{\delta(k_2)\cdot k_2 \cdot V_{\text{dck,ca}}}{\text{imag}(Z\text{ca, 2nd})\cdot I_{\text{max,ba}}}\right) \end{aligned} \tag{9}$$

where

$$\sigma = \frac{(2\theta_b + \sin 2\theta_b) - 4\beta_{\text{bo}}\sin\theta_b}{2\pi(1-\beta_{\text{bo}})}. \tag{10}$$

Combining formula (7), the reactance of BA can be expressed as

$$\left(-j \cdot \frac{\sqrt{2}}{3\pi}\cdot\frac{1}{\sigma}\cdot\frac{I_{\text{max,ca}}}{I_{\text{max,ba}}}, j \cdot \frac{\sqrt{2}}{3\pi}\cdot\frac{1}{\sigma}\cdot\frac{I_{\text{max,ca}}}{I_{\text{max,ba}}}\right). \tag{11}$$

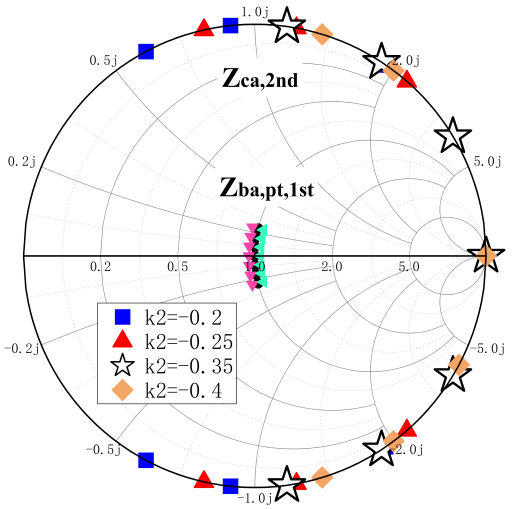

FIGURE 3. BA fundamental impedance and CA second harmonic impedance under different k_2 conditions

According to (9) and (11), the fundamental port impedance of the BA can be expanded not only resistively but also reactively on the Smith chart, as shown in Fig. 3. By appropriately controlling the second harmonic impedance $Z_{\text{ba,pt,2nd}}$ in the BA port, optimal peak power level performance can be achieved in terms of efficiency and output power. Since the fundamental port impedance of the BA naturally tracks the design space of the B/J-class operating mode, the second harmonic impedance $Z_{\text{ba,pt,2nd}}$ at the BA port should be appropriately tuned according to J-class theory such that

$$Z_{\text{ba,pt,2nd}} = -j \cdot \frac{3\pi}{8}\delta, |\delta| \le \delta_{\max} \tag{12}$$

where $\delta_{\max}$ is the parameter of the CM design space that controls the second harmonic design of the BA class J. By substituting (9) and (11) into (12), $\delta_{\max}$ can be calculated and expressed as

$$\begin{aligned} \delta_{\max} &= \frac{\left|\frac{\sqrt{2}}{3\pi}\cdot\frac{1}{\sigma}\cdot\frac{I_{\text{max},ca}}{I_{\text{max},ba}}\right|}{1 + \sqrt{2}\left(\frac{1}{2} - \frac{8}{9\pi^2}\right)\cdot\frac{1}{\sigma}\cdot\frac{I_{\text{max},ca}}{I_{\text{max},ba}}} \\ &= \frac{1}{\frac{3\pi}{\sqrt{2}}\cdot\frac{(2\theta_b + \sin 2\theta_b) - 4\beta_{\text{bo}}\sin\theta_b}{2\pi(1-\beta_{\text{bo}})}\frac{I_{\text{max,ba}}}{I_{\text{max,ca}}} + \left(\frac{3\pi}{2} - \frac{8}{3\pi}\right)} \end{aligned} \tag{13}$$

From the above analysis, it can be concluded that the design space of both the CA and BA can be expanded while maintaining excellent performance in terms of efficiency and output power.

3. DESIGN OF THE PROPOSED SLMBA

To validate the proposed theory, an RF input SLMBA using gallium nitride (GaN) transistors was designed and fabricated with a target bandwidth of 2–3.7 GHz to cover the 5G New Radio (NR) frequency band. Wolfspeed's 10 W GaN HEMT (CG2H40010F) was used as the active device for both CA and

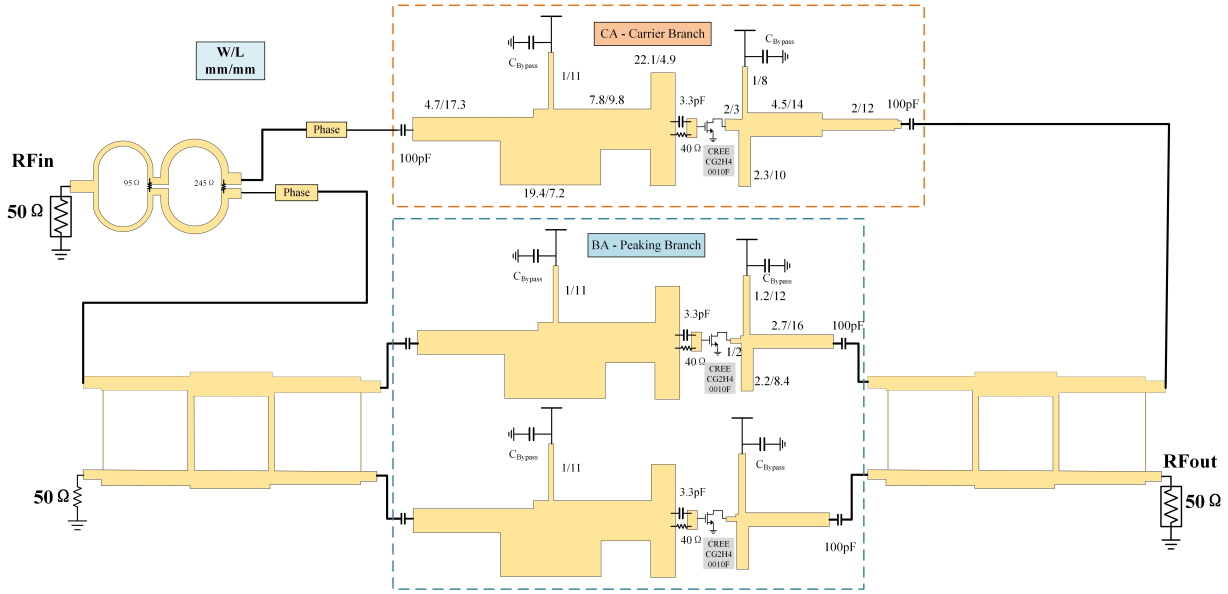

FIGURE 4. Schematic of the proposed SLMBA.

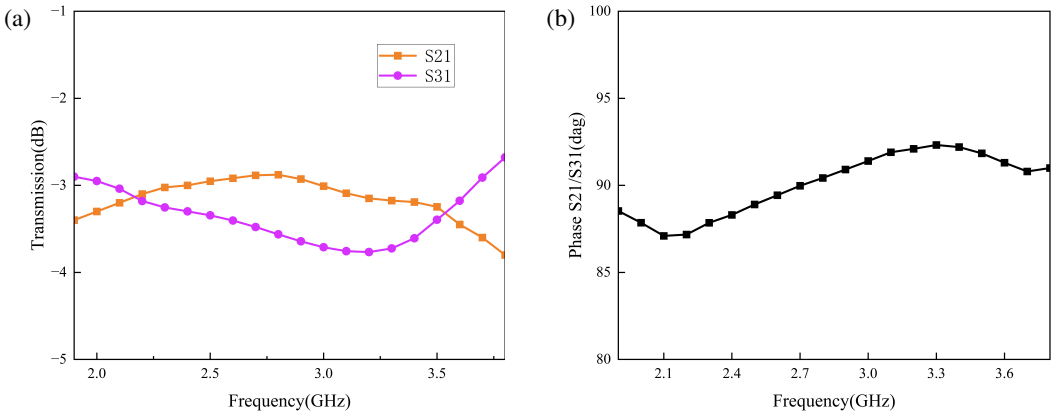

FIGURE 5. EM simulation results of the designed broadband coupler. (a) Transmission. (b) Phase difference between ports 2 and 3.

BA. The SLMBA was implemented on a Rogers 4350B substrate with a thickness of 30 mil and a dielectric constant of 3.48. Using an input threshold of $\beta_{bo} = 0.5$, the target was set to an 8 dB output power back-off (OPBO) level.

Since the CA and BA amplifiers use identical transistors, the CA was matched to a larger load impedance and supplied with a reduced drain voltage to decrease its output power and thereby achieve the target power back-off. The CA was designed to deliver approximately 38 dBm of saturated output power in the OBO, while the BA used a higher drain voltage to achieve approximately 46 dBm of saturated output power.

The SLMBA design procedure consists of the following steps: 1) Design a broadband 3-dB orthogonal coupler; 2) Design the output matching network (OMN) for the CA operating in continuous F^{-1} mode; 3) Design the OMN for the BA; 4) Design the input matching networks (IMN) for CA and BA; 5) Design a phase shift network (PSN) to compensate for the phase difference between CA and BA, enabling the LMBA to achieve high output power and efficiency. A schematic diagram of the proposed SLMBA is shown in Fig. 4.

3.1. Design of the Coupler

The CA load impedance is designed to exceed 50 Ω. The BA load impedance is designed at 32 Ω, which is the optimal load impedance for transistors operating in Class B mode. Considering all factors comprehensively, the characteristic impedance of the coupler is designed at 50 Ω and applied to the input and output terminals of the proposed SLMBA. To achieve coupler performance within the 2–3.7 GHz target frequency band, a three-stage stub-line hybrid structure was adopted for the coupler design. Fig. 5(a) shows the S-parameter results from the electromagnetic simulation of the designed coupler, while Fig. 5(b) displays the phase difference at the coupler's output port. It can be observed that the transmission parameters are close to the ideal values, with the phase difference remaining nearly constant at 90 degrees.

3.2. Design of the Broadband Continuous Class-F-1 CA

Based on the theoretical analysis presented in Section 2, the fundamental current component function of the CA, expressed

as a second harmonic reactance, requires an expanded variation, with the second harmonic reactance curve lying in the open-circuit region of the Smith chart. Therefore, the CA operates in reverse F-class mode. The parasitic and packaging parameters in commercial transistors usually limit access to the intrinsic plane of the device. In order to extract the intrinsic drain current and voltage as well as the intrinsic impedance, the de-embedded network of the CG2H40010F transistor was used in the actual OMN design [19, 20]. Load-pull simulations were performed using the de-embedded model, selecting the appropriate intrinsic fundamental impedance of the transistor. To achieve good inverse F-class impedance matching performance, matching was performed using the embedded model and fundamental intrinsic impedance, while co-designing with the coupler. The output port of the OMN is connected to the designed coupler as shown in Fig. 6. The intrinsic trajectories are shown in Fig. 7. The topology and parameters of the CA OMN are shown in Fig. 4. After designing the CA OMN, the IMN is designed based on the CA input impedance. The topology and parameters of the CA IMN are shown in Fig. 4. A 100-pF capacitor is used for DC blocking. A 40-Ω resistor and a 3.3-pF capacitor form an RC parallel circuit, ensuring the stability of the transistor.

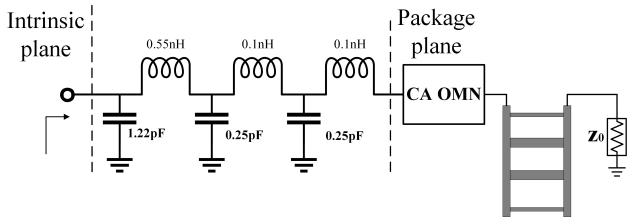

FIGURE 6. **CA OMN:** Co-design with coupler.

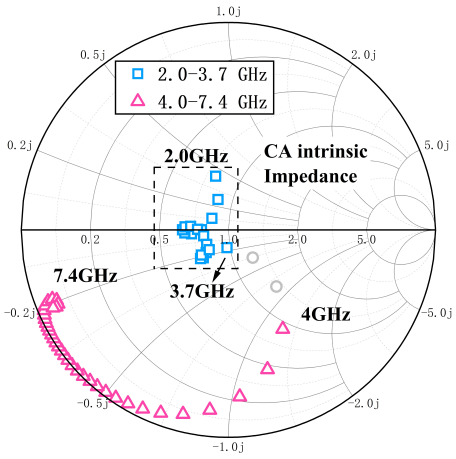

FIGURE 7. Design the impedance of the CA load matching network on the Smith chart with reference impedance 50.

3.3. Design of the Broadband BAs

To achieve a saturated output power of 46 dBm, each BA must output 43 dBm of power when saturated. In this case, the BA drain voltage is set to 36 V, and the load impedance is approximately 32 Ω. Similarly to the CA OMN design, the BA OMN design also utilized the de-embedded network to achieve both intrinsic and extrinsic impedance trajectories, with the intrinsic impedance trajectory shown in Fig. 8. The port impedance of the BA as seen from the coupler port is converted into the load modulation trajectory on the real axis of the transistor's intrinsic impedance. The topology and parameters of the BA OMN are shown in Fig. 4.

3.4. Design of the Wideband PSN

The final and critical step in the complete SLMBA design procedure involves the design and implementation of the phase shift network (PSN). This network is essential for compensating the phase discrepancy between the carrier amplifier (CA) and the balanced amplifier (BA) paths, ensuring coherent power combination at the output coupler and thus maximizing overall output power and efficiency. The design methodology is carried out systematically in two primary stages. First, an ideal phase shift network is employed in simulation to determine the precise optimal phase shift value required at each corresponding frequency point across the target operating band (2.0–3.7 GHz). This ideal network provides a theoretical benchmark for phase compensation performance. Subsequently, this ideal phase shift value is converted into a practical implementation using a physical transmission line segment. The electrical length and characteristic impedance of this transmission line are carefully calculated to realize the desired phase shift across the bandwidth, thereby completing the design of the PSN and enabling the LMBA to achieve high-efficiency performance.

3.5. Simulation Results

The complete circuit schematic of the proposed SLMBA is shown in Fig. 4. Electromagnetic (EM) simulation was performed using Advanced Design System (ADS) software. The selected intrinsic load modulation trajectories of the BA at different frequencies are shown in Fig. 9, which aligns with the design theory at saturation power levels depicted in Fig. 3. Additionally, Figs. 10(a)–10(c) display the BA intrinsic current and voltage waveforms of the BA at 2, 2.6, and 3.1 GHz when the proposed SLMBA operates in saturation mode. We can observe that the BA peak branch is functioning in a typical harmonic-controlled mode. Fig. 11 displays the simulated drain efficiency (DE) and gain versus the output power for the proposed SLMBA across 2.0–3.7 GHz in 0.2 GHz. The simulation results indicate peak power efficiency ranging from 60.3% to 75.2%, with saturated output power levels of 45.2–46.1 dBm. At an OBO back-off level of 8 dB, the DE ranges from 49.5% to 63.1%. A gain of 9.6–11.6 dB is achieved at an output power level of approximately 28 dBm, highlighting the excellent broadband performance of the designed SLMBA within the target frequency band.

4. EXPERIMENTAL RESULTS

Figure 12 shows a photograph of the actual test board, which measures 221 mm × 114 mm. During measurement, the CA was biased at a drain supply voltage of 20 V. The drain and gate voltages of the peak amplifier (BA) were set to 36 V and −5 V, respectively. The small-signal characteristics of the designed

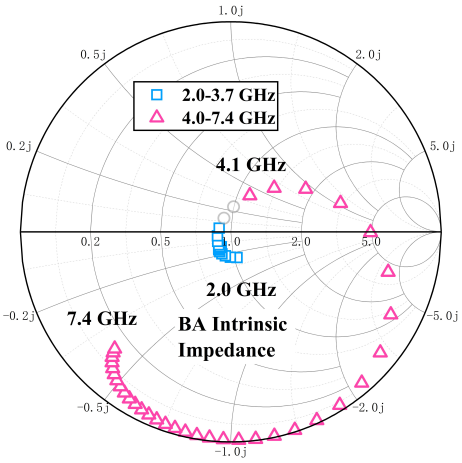

FIGURE 8. Design the impedance of the BA load matching network on the Smith chart with reference impedance 50.

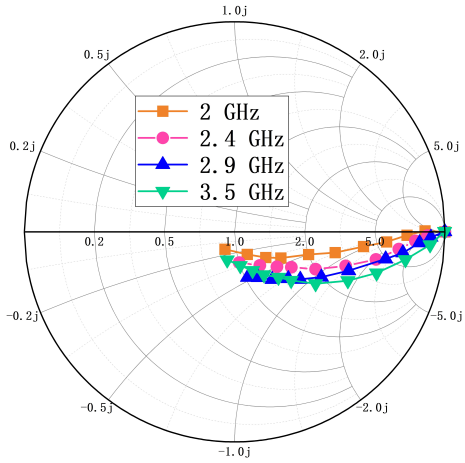

FIGURE 9. Simulated load modulation trajectories of BA intrinsic impedance Z_{ba} at selected frequency points.

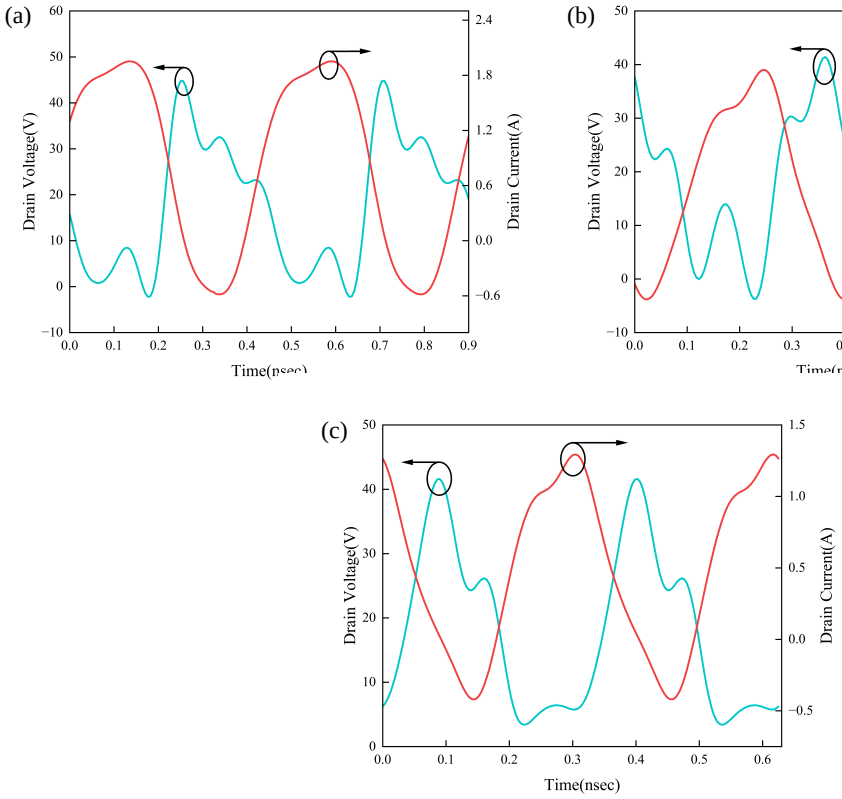

FIGURE 10. BA simulation results at 1.9, 2.2, and 2.5 GHz at saturation in the entire W-SLMBA. (a)–(c) Drain current and voltage waveforms.

SLMBA were first measured using a vector network analyzer to evaluate its linearity and stability in preparation for subsequent large-signal tests. A continuous-wave (CW) signal was used to conduct large-signal measurements on the fabricated PA. The CW signal was generated by a signal generator, and the output power was measured using a spectrum analyzer. A linear driver amplifier was employed to ensure sufficient input power to the device under test, and an isolator was inserted between the driver amplifier and the test board to improve isolation. Owing to manufacturing tolerances and model inaccuracies, the measured results exhibited slight deviations from the simulated performance across the frequency band. Fig. 13 illustrates the measured drain efficiency (DE) and gain versus output power at multiple frequencies. As shown in Fig. 14, the relationship between PAE and output power measured at different operating frequencies is presented, enabling a better power evaluation. Furthermore, to better demonstrate broadband performance, Fig. 15 presents the measured DE and gain at various levels of output power, as well as the saturated output power as a function of frequency.

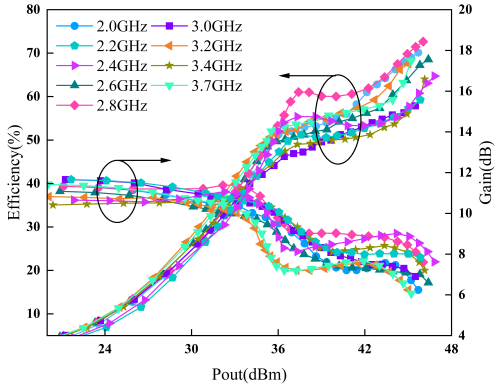

FIGURE 11. Simulated DE and gain versus output power over 2–3.7 GHz.

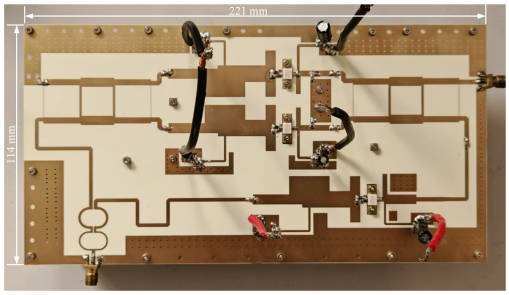

FIGURE 12. Photograph of the fabricated SLMBA.

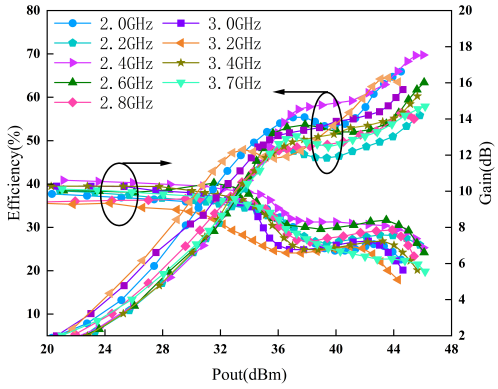

FIGURE 13. Measured DE and gain versus output power over 2–3.7 GHz.

Within the achieved bandwidth, the proposed SLMBA delivered a peak DE of 55.2%–68.7% at a saturated output power ranging from 44.1 to 45.1 dBm. Across the entire operating band, at an 8 dB output power back-off (OPBO), DE values between 46.8% and 59.0% were attained. At an output power level of approximately 28 dBm, the gain varied from 8.2 to 10.2 dB. The proposed SLMBA achieves a fractional bandwidth of 59%. To evaluate the linearity and efficiency under modulated excitation, a 100 MHz Long Term Evolution (LTE) signal with a peak-to-average power ratio (PAPR) of 8 dB was used to test the SLMBA in the 2.0–3.7 GHz band. Fig. 16

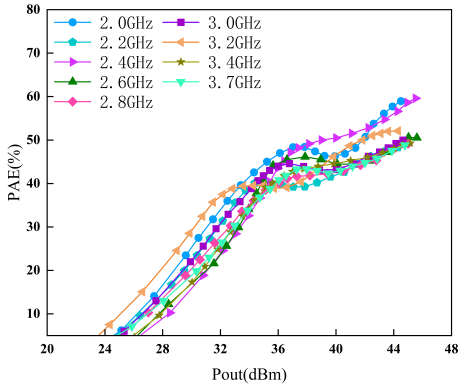

FIGURE 14. Measured PAE versus output power over 2-–3.7 GHz.

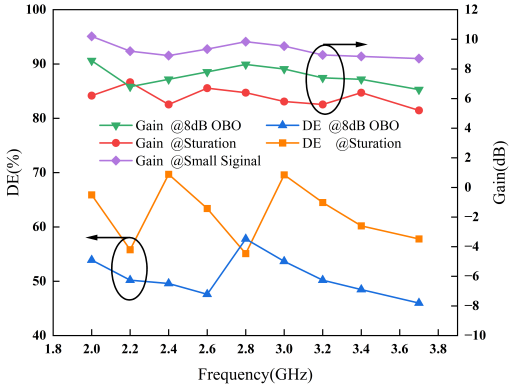

FIGURE 15. Measured DE and gain versus frequency with CW signal test.

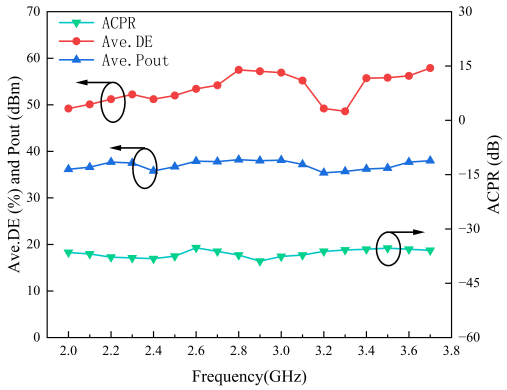

FIGURE 16. Relationship between average DE, output power, and ACPR versus frequency, measured under a 100-MHz 8-dB PAPR LTE signal test at 2.0–3.7 GHz.

shows the measured average drain efficiency, output power, and adjacent channel power ratio (ACPR) across the band under modulated excitation. Experimental results indicate that the fabricated SLMBA achieves an average output power of 35.8–38.2 dBm with an average drain efficiency exceeding 49.2%.

Table 1 summarizes the performance of various recently reported LMBA and SLMBA architectures. The comparative

TABLE 1. Performance comparison of recently published load modulated PAS.

Ref. (Year)	Technique N/A	Freq. (GHz)	BW. (GHz/%)	Pmax (dBm)	Gain (dB)	OPBO (dB)	DE @OPBO (%)	DE @Pmax (%)
[3] 2018	CM-DPA	1.6–2.7	1.1/51	43.8–45.2	9.4–11.5	6	46.5–63.5	56–75.3
[20] 2019	DEPA	2.5–3.8	1.25/40	48.8–49.8	9.3–12.7	8	47–60	54–67
[8] 2017	RF-Input LMBA	1.8–3.8	2.0/71	42–44	11–12	6	33–49	46–70
[12] 2020	RF-Input PD-LMBA	1.5–2.7	1.2/57	43	8	6/10	47–61/ 47–58	58–72
[10] 2020	RF-Input SLMBA	3.05–3.55	0.5/15.2	42.3–43.7	9.5–10.3	6/8/10	50.9–64.9/ 46.8–60.7/ 43.2–51.4	60.8–74.8
[16] 2021	RF-Input H-ALMBA	1.7–3.0	1.3/55	42–43	8–13	6/10	50–61/ 50–56	63–81
[21] 2025	LMBA	1.7–1.9	0.2/11	46–47	14.8–17.1	6	40.5–46.8	60–63
[22] 2023	2-stage-CSA	3.3–3.8	0.5/14	45	7.5–12.2	7.5	47–52	55–63
This work	RF-Input SLMBA	2.0–3.7	1.7/59	44.7–46.5	9.1–10.6	8	46.8–59	55.2–68.7

results show that the proposed SLMBA offers superior efficiency under both saturated and 8-dB output back-off (OBO) conditions. This RF-input SLMBA achieves broad bandwidth while maintaining a higher back-off efficiency than other published LMBA designs. Compared to Doherty power amplifiers (DPAs) employing the same continuous-mode (CM) technology, the proposed SLMBA achieves a larger back-off range with comparable efficiency.

5. CONCLUSION

This study proposes an improved sequential load-modulated balanced amplifier (SLMBA). Its core principle is based on continuous F^{-1} class theory, which utilizes changes in the second harmonic load reactance of the carrier amplifier (CA) to regulate the fundamental current component it injects, thereby expanding the load modulation design space of the balanced amplifier (BA) and enhancing its back-off efficiency characteristics. To validate this theory, a broadband SLMBA operating in the 2–3.7 GHz frequency band was designed and fabricated. Simulation results confirm that the theoretical derivations align with the BA load modulation trajectory. Measurement results within the 2.0–3.7 GHz frequency band indicate that the amplifier achieves a drain efficiency (DE) of 55.2%–68.7% at 8-dB output power back-off (OPBO) and 46.8%–59.0% at 45.1-dBm peak power.

ACKNOWLEDGEMENT

This work was supported by the Liaoning key Laboratory of Radio Frequency and Big Data for Intelligent Application (2021JH13/10200055).

REFERENCES

[1] Lien, S.-Y., S.-L. Shieh, Y. Huang, B. Su, Y.-L. Hsu, and H.-Y. Wei, "5G new radio: Waveform, frame structure, multiple access, and initial access," *IEEE Communications Magazine*, Vol. 55, No. 6, 64–71, 2017.

[2] Shafi, M., A. F. Molisch, P. J. Smith, T. Haustein, P. Zhu, P. D. Silva, F. Tufvesson, A. Benjebbour, and G. Wunder, "5G: A tutorial overview of standards, trials, challenges, deployment, and practice," *IEEE Journal on Selected Areas in Communications*, Vol. 35, No. 6, 1201–1221, 2017.

[3] Shi, W., S. He, X. Zhu, B. Song, Z. Zhu, G. Naah, and M. Zhang, "Broadband continuous-mode Doherty power amplifiers with noninfinity peaking impedance," *IEEE Transactions on Microwave Theory and Techniques*, Vol. 66, No. 2, 1034–1046, 2018.

[4] Shepphard, D. J., J. Powell, and S. C. Cripps, "An efficient broadband reconfigurable power amplifier using active load modulation," *IEEE Microwave and Wireless Components Letters*, Vol. 26, No. 6, 443–445, 2016.

[5] Shepphard, D. J., J. Powell, and S. C. Cripps, "A broadband reconfigurable load modulated balanced amplifier (LMBA)," in *2017 IEEE MTT-S International Microwave Symposium (IMS)*, 947–949, Honolulu, HI, USA, 2017.

[6] Quaglia, R. and S. Cripps, "A load modulated balanced amplifier for telecom applications," *IEEE Transactions on Microwave Theory and Techniques*, Vol. 66, No. 3, 1328–1338, 2018.

[7] Pednekar, P. H. and T. W. Barton, "RF-input load modulated balanced amplifier," in *2017 IEEE MTT-S International Microwave Symposium (IMS)*, 1730–1733, Honolulu, HI, USA, 2017.

[8] Pednekar, P. H., E. Berry, and T. W. Barton, "RF-input load modulated balanced amplifier with octave bandwidth," *IEEE Transactions on Microwave Theory and Techniques*, Vol. 65, No. 12, 5181–5191, 2017.

[9] Pednekar, P. H., W. Hallberg, C. Fager, and T. W. Barton, "Analysis and design of a Doherty-like RF-input load modulated bal-

anced amplifier," *IEEE Transactions on Microwave Theory and Techniques*, Vol. 66, No. 12, 5322–5335, 2018.

[10] Pang, J., Y. Li, M. Li, Y. Zhang, X. Y. Zhou, Z. Dai, and A. Zhu, "Analysis and design of highly efficient wideband RF-input sequential load modulated balanced power amplifier," *IEEE Transactions on Microwave Theory and Techniques*, Vol. 68, No. 5, 1741–1753, 2020.

[11] Pang, J., C. Chu, Y. Li, and A. Zhu, "Broadband RF-input continuous-mode load-modulated balanced power amplifier with input phase adjustment," *IEEE Transactions on Microwave Theory and Techniques*, Vol. 68, No. 10, 4466–4478, 2020.

[12] Cao, Y. and K. Chen, "Pseudo-Doherty load-modulated balanced amplifier with wide bandwidth and extended power backoff range," *IEEE Transactions on Microwave Theory and Techniques*, Vol. 68, No. 7, 3172–3183, 2020.

[13] Cao, Y., H. Lyu, and K. Chen, "Asymmetrical load modulated balanced amplifier with continuum of modulation ratio and dual-octave bandwidth," *IEEE Transactions on Microwave Theory and Techniques*, Vol. 69, No. 1, 682–696, 2021.

[14] Colantonio, P., F. Giannini, G. Leuzzi, and E. Limiti, "High efficiency low-voltage power amplifier design by second-harmonic manipulation," *International Journal of RF and Microwave Computer-Aided Engineering*, Vol. 10, No. 1, 19–32, 2000.

[15] Chu, C., T. Sharma, S. K. Dhar, R. Darraji, X. Wang, J. Pang, and A. Zhu, "Waveform engineered sequential load modulated balanced amplifier with continuous class-F-1 and class-J operation," *IEEE Transactions on Microwave Theory and Techniques*, Vol. 70, No. 2, 1269–1283, 2021.

[16] Cao, Y., H. Lyu, and K. Chen, "Continuous-mode hybrid asymmetrical load-modulated balanced amplifier with three-way modulation and multi-band reconfigurability," *IEEE Transactions on Circuits and Systems I: Regular Papers*, Vol. 69, No. 3, 1077–1090, 2022.

[17] Chu, C., J. Pang, R. Darraji, S. K. Dhar, T. Sharma, and A. Zhu, "Broadband sequential load modulated balanced amplifier with extended design space using second harmonic manipulation," *IEEE Transactions on Microwave Theory and Techniques*, Vol. 71, No. 5, 1990–2003, 2023.

[18] Colantonio, P., F. Giannini, and E. Limiti, *High Efficiency RF and Microwave Solid State Power Amplifiers*, John Wiley & Sons, 2009.

[19] Jang, H., P. Roblin, and Z. Xie, "Model-based nonlinear embedding for power-amplifier design," *IEEE Transactions on Microwave Theory and Techniques*, Vol. 62, No. 9, 1986–2002, 2014.

[20] Saad, P., R. Hou, R. Hellberg, and B. Berglund, "The continuum of load modulation ratio from doherty to traveling-wave amplifiers," *IEEE Transactions on Microwave Theory and Techniques*, Vol. 67, No. 12, 5101–5113, 2019.

[21] Mehter, E. and M. Üçüncü, "Radio frequency (RF) power amplifier design providing high power efficiency in a wide dynamic range," *Electronics*, Vol. 14, No. 7, 1435, 2025.

[22] Mochumbe, S. E. and Y. Yang, "Design of a load modulated balanced amplifier with a two-stage control power amplifier," *Journal of Electromagnetic Engineering and Science*, Vol. 23, No. 3, 294–301, 2023.